International Journal of Advance and Innovative Research
Volume 12, Issue 2 (XXII): April - June 2025
ISSN 2394 - 7780

APPLICATION OF HYBRID SIMULATION TO THE CRYOSURGERY OF AN IRREGULAR TUMOR

Dr. Rama Bhargava
Pro Vice Chancellor, Haridwar University Roorkee

ABSTRACT
In the current paper, numerical simulation has been done for the two-dimensional time dependent Pennes' heat transfer model, solved for irregular diseased tumor cells. An elliptic cryoprobe of varying sizes is taken at the center of the computational domain in such a manner that the location of the probe is fixed throughout the computation. The cooling performance of various nanoparticles injected at very low temperature, has been studied by implementing hybrid FEM/EFGM approach. Rate of cooling is obtained for various nanoparticles and infusion of Au nanoparticles is highly efficient on increasing the heating rate than other nanoparticles.

INTRODUCTION
Cryosurgery is one of the oldest and simplest ways to treat the injuries. Because of its low cost, convenience, effectiveness and ease of transportation; this treatment has become very efficient. During surgery, the probe is inserted at very low temperature to freeze the tumor cells through convection. Many researchers have worked to increase the efficiency of the surgery by implementing various conditions during treatment. Liu and Deng [1] studied the nano-cryosurgery treatment of the tumor tissue in which infusion of the nanoparticles is helpful in maximizing the freezing process and reducing the freezing of the healthy tissues. infusion of the nanoparticles during surgery. Hou et al. [2] implemented the nano-cryosurgery treatment for the tumor tissues using MgO, Fe_3O_4, Ag, and Al_2O_3 nanoparticles.

In order to increase the efficiency, researchers have worked on various numerical scheme to study the rate of cooling during surgery. Rui et al. [3], Zhang et al. [4], Zhao et al. [5], He et al. [6], and Tanwar et al. [7] implemented finite element scheme for the simulation of bioheat equation to study the phase transition during cryosurgery. Further simulation was done by Singh and Bhargava [8] for the Cryosurgical treatment of tumor tissues using meshfree approach. Number of probes used during surgery is helpful in increasing the efficiency of the treatment. Rabin and Steif solved the bioheat equation by assuming the spherical cryoprobe.

The run time of simulation in surgery has become one of the important parameters to study. Tanaka et al. [9] proposed two-phase optimization scheme in which phase I is based on finite elements meshing and phase II is based on force-field analogy method.

In this paper, an elliptic probe is used for the cryosurgery, with Hybrid approach. Results are validated and the accuracy is checked. To make results more acceptable, they are compared with actual surgery details.

PROBLEM FORMULATION
A two-dimensional unsteady bio-heat transfer model has been taken inside a square domain (Ω) of 10×10 cm^2 unit which contains an irregular diseased tumor. An elliptic probe (P) of varying sizes with infusion of different nanoparticles Au, Al O2 3, Fe O3 4, has been introduced at the center of the tumor. The temperature of the probe is fixed throughout the computation. The hybrid FEM/EFGM method is implemented for simulation of time dependent partial differential equation in which the computational domain is decomposed into two subdomains, that is, EFGM domain which is meshfree domain and FEM domain which is mesh based domain.

2.1. Mathematical Model
The two-dimensional form of unsteady bio-heat transfer model proposed by Pennes' [10] is given as follows:

$$(pc)eff\frac{\partial T}{\partial t} = k_{eff}\left(\frac{\partial^2 T}{\partial X^2} + \frac{\partial^2 T}{\partial Y^2}\right) + \omega_b \rho_b c_b (T_b - T) + Q_m - Q. \quad (1)$$

On infusion of the nanoparticles, heat transfer model is reduced in the following form:

$$((pc)nf)_{eff}\frac{\partial T}{\partial t} = (k_{nf})_{eff}\nabla^2 T + \omega_b \rho_b c_b (T_b - T) + Q_m - Q. \quad (2)$$

ISSN 2394 - 7780

The domain of the probe P is given as follows:

$$\Gamma_p : \frac{X^2}{a^2} + \frac{Y^2}{b^2} \leq 1, \qquad (3)$$

NUMERICAL SIMULATION

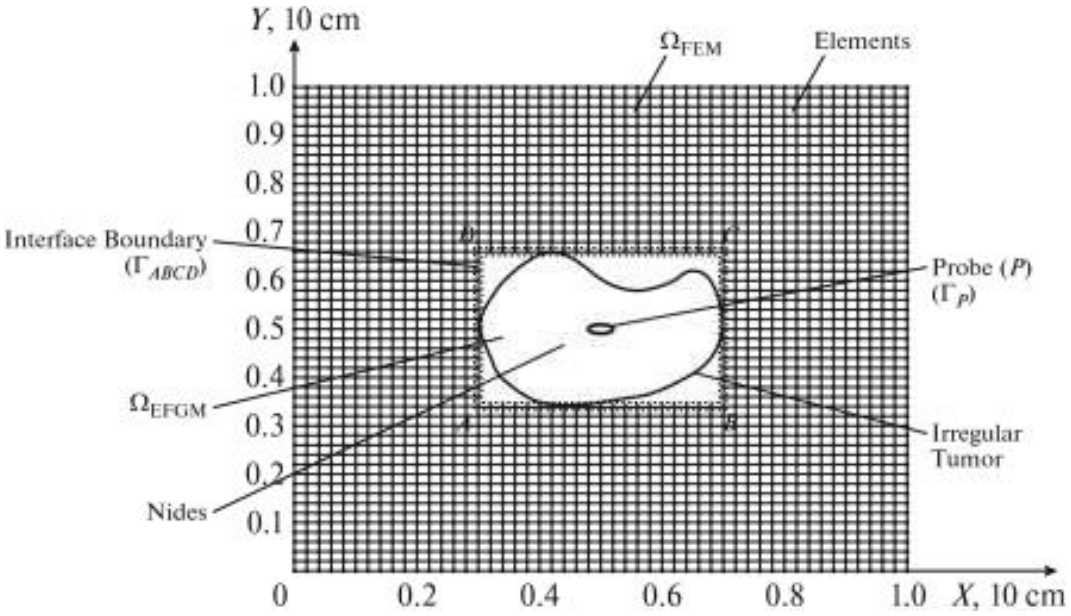

Various constants depend on the temperatures of the lower phase change (T_S) and the upper phase change (Tl).

The effective heat capacity for the frozen and unfrozen tissues is taken as

$$(pc)_{frozen} = T < T_s$$

$$(pc)_{eff} = \frac{(pc)_{frozen} + (pc)_{unfrozen}}{2} + \frac{p\hbar}{i \quad s}, T_s \leq T \leq T_i$$

$$(pc)_{unrozen,} = T < T_i$$

The effective thermal conductivity for the frozen as well as unfrozen tissues has been considered as

$$(k)_{frozen} = T < T_s$$

$$(k)_{eff} = \frac{(k)_{frozen} + (k)_{unfrozen}}{2} + T_s \leq T \leq T_i$$

$$(k)_{unrozen,} = T < T_i$$

The heat capacitance for the nanofluid is given by

$(\rho c)nf = (1 - \phi(\rho c)f + \phi(\rho c)s$

The density of the nanofluid is taken as

$\rho_{nf} = (1 - \phi)p_f + \phi\rho s.$

SOLUTION METHOD

The size and shape of the probe can be varied depending on the shape of the diseased tumor cells. An elliptic probe with infusion of different nanoparticles Au, Al O2 O 3, Fe3 O4, has been injected at the center of the ΩEFGM. For ΩEFGM, the shape function is constructed at each step during analysis while for ΩFEM, the shape function is predefined for a particular type of element which is fixed throughout the computation. Here rectangular element is used in ΩFEM for simulation, with shape functions as below:

ISSN 2394 - 7780

$$N_1 = \frac{1}{4}(1-\xi)(1-\eta), N_2 = \frac{1}{4}(1+\xi)(1-\eta),$$
$$N_3 = \frac{1}{4}(1-\xi)(1-\eta), N_4 = \frac{1}{4}(1+\xi)(1-\eta).$$

Where the Jacobian matric (J) is given by

$$|J| = \begin{bmatrix} \frac{\partial X}{\partial \xi} & \frac{\partial Y}{\partial \xi} \\ \frac{\partial X}{\partial \eta} & \frac{\partial Y}{\partial \eta} \end{bmatrix}$$

In Ω_{EFGM}, the shape function is approximated by moving least square approximation in which the shape changes with change in location at each step during analysis where the field variable for the EFGM domain is given by

$$T(X,Y) = T^h(X) = \sum_{I=1}^{4} \emptyset_I(X) T_I.$$

It is a linear basis function of order 3 in two dimension and *N* is the number of nodes scattered in Ω_{EFGM}.

The problem domain is $\Omega = \Omega_{EFGM} \cup \Omega_{FEM}$ with 51 × 51 nodes scattered throughout the domain in which the two decomposed domains are separate by the interface boundary Γ_{ABCD}. The interface boundary contains the nodes of the domain Ω_{EFGM} as well as the nodes of the elements of Ω_{FEM}. At the interface boundary, the vector

$$\boldsymbol{p}(\boldsymbol{X}) = \sum_{J=1, XJ \in \Gamma I} p(\boldsymbol{XJ}) \phi I(\boldsymbol{X}) + \sum_{MJ=1, XJ \in \Gamma I} p(\boldsymbol{XJ}) NJ(\boldsymbol{X})$$

$$\text{which gives } \boldsymbol{p}(\boldsymbol{X}) = \boldsymbol{A}(\boldsymbol{X})\boldsymbol{a}(\boldsymbol{X}) + \sum_{J=1, X_I \in \Gamma_I}^{M} p(\boldsymbol{X}_I) N_I(\boldsymbol{X})$$

vector $\boldsymbol{a}(\boldsymbol{X}) = \{\boldsymbol{p}(\boldsymbol{X}) - \sum_{J=1, X_I \in \Gamma_I}^{M} p(\boldsymbol{X}_I) N_I(\boldsymbol{X})\}^T \boldsymbol{A}^{-1}(\boldsymbol{X})$, is evaluated at every node.

The domain Ω_{EFGM} is defined as follows:

$$\Omega EFGM: \quad 0.3 \leq \leq X \ 0.7$$
$$0.34 \leq \leq Y \ 0.66.$$

Moreover, the remaining domain is confined with Ω_{FEM} which is defined as follows:

$$\Omega_{FEM}: \quad (0 \leq X \leq 1) - (0.3 < X < 0.7)$$
$$(0 \leq Y \leq 1) - (0.34 < Y < 0.66).$$

Both the domains contain the nodes of the interface boundary Γ_{ABCD}, for which the shape function is defined accordingly. The details of all of these can be seen from (8). The variational formulation is.

$$\int_{\Omega_e} W \left[(\rho c)_{eff} \frac{\partial T}{\partial t} - k_{eff} \left(\frac{\partial^2 T}{\partial X^2} + \frac{\partial^2 T}{\partial Y^2} \right) - \omega_b \rho_b c_b (T_b - T) - Q_m + Q \right] d\Omega_e = 0$$

The reduced weak form of above formulation is

$$\int_{\Omega_e} \left[W(\rho c)_{eff} \frac{\partial T}{\partial t} + k_{eff} \left(\frac{\partial W}{\partial X}\frac{\partial T}{\partial X} + \frac{\partial W}{\partial Y}\frac{\partial T}{\partial Y} \right) + \omega_b \rho_b c_b W T \right] d\Omega_e$$
$$= (\omega_b \rho_b c_b T_b + Q_m - Q) \int_{\Omega_e} W d\Omega_e$$

The above are now famulated at each node which are finally reduced to a system of equations to be solved using our own coding. The results are shown graphically.

ISSN 2394 - 7780

Table 1. Thermo-physical properties of nanoparticles and biological tissues

Symbol	Quantity	Value (in units)
ωb ρf ρu ρb	Blood perfusion rate	0.0005 ml/s/ml
ρp(Au) ρp(Al O2 3)	Density of frozen tissue	1000 Kg/m^3
ρp(Fe O3 4)	Density of unfrozen tissue	1000 Kg/m^3
	Density of blood Density of Au	1000 Kg/m^3
		19320 Kg/m^3
$\bar{h}$ Qm' cf cu	Density of Al O23	3970 Kg/m^3
cp(Au) cp(Al2O3)	Density of Fe O34 Latent heat	4800 Kg/m^3
cp(Fe3O4) Ts	Metabolic rate of liver Specific heat capacity of frozen tissue	4.2 × 10^6 J/Kg
Tl k	Specific heat capacity of unfrozen tissue Specific heat capacity	4200 W/m^3
f ku	of Au	1.8 × 10^3 J/m^3 °C
kp(Au) kp(Al2O 3)		3.6 × 10^3 J/m^3 °C
kp(Fe3O 4)	Specific heat capacity of Al O23	2.21 × 10^3 J/m^3 °C
	Specific heat capacity of Fe O34 Temperature of lower phase	2.82 × 10^3 J/m^3 °C
	change Temperature of upper phase change Thermal	3.2 × 10^3 J/m^3 °C
	conductivity of frozen tissue Thermal conductivity of unfrozen	−8°C
	tissue Thermal conductivity of Au	−1°C
	Thermal conductivity of Al O23	2.0 W/m °C
	Thermal conductivity of Fe O34	0.5 W/m °C
		297.7 W/m °C
		39.7 W/m °C
		7.1 W/m °C

RESULTS AND DISCUSSION

The cryoprobes are kept at very low temperature to freeze the infected tumor tissues. The capability of the probe to diagnose the unhealthy tissues depends on shape, size as well as position of the probe. The size and growth of the probe formed during freezing process are controlled by nanoparticle volume fraction. From the existing literature and experimental results, the critical temperature is figured out to be –40°C to –50°C which is that much adequate to kill the tumor tissues.

The infusion of different nanoparticles Au, Al2O 3, Fe3O4 are taken into picture. The diameter of the nanoparticles d_p is taken as 10 nm, nanoparticle concentration ϕ is 20% and conductivity ratio for the base fluid to the nanolayer is taken as 20. The cooling rate of the probe is 7.2 × 10^{-7} W/m^3 s which is kept constant throughout the computation. The thermo- physical properties of the nanoparticles as well as the biological tissue are given in Table 1.

Figure 1 describes temperature contours inside the computational domain for the Gold (Au) nanoparticles. The cooling rate of the tissue is higher near the center of the probe. On moving away from the center of the probe, the temperature varies slightly which is nearly unchanged at the positions far away from the probe. After 20 minutes of freezing, the size of the cryoprobe formed in the diagnosed region has increased. After 15 minutes of cooling process, the temperature of the tissue for the Gold (Au) nanoparticles at 14 mm away from center of the probe along semi minor axis is approximately –46.21°C which is varied to –23.47°C at 18 mm away from center of the probe along semi minor axis (Table 2). Some are computed with other nanoparticles and the results are shown in Fig. 2, 3, 4.

ISSN 2394 - 7780

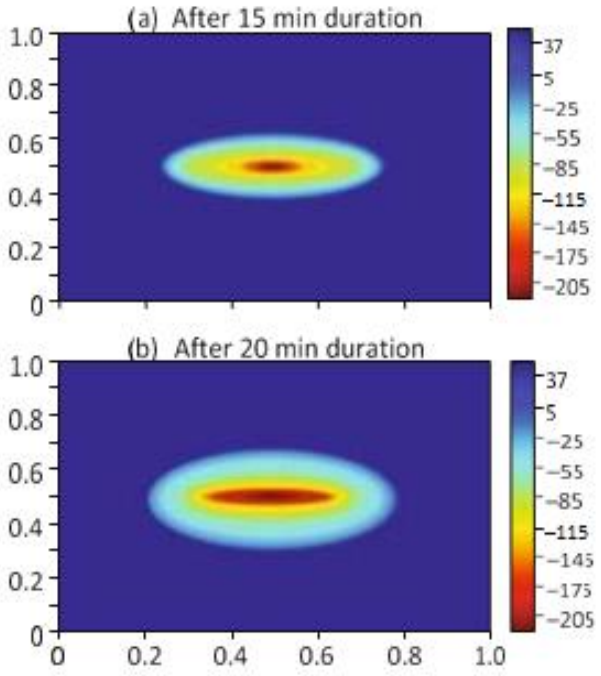

Fig. 1. Temperature Profile inside the computational domain for Au nanoparticles at 4 mm major axis and 2 mm minor axis of cryoprobe for $\phi = 0.20$, $dp = 10$ nm and $\delta = 20$.

Table 2. Comparison of temperature for different nanoparticles at various points away from center of the probe

Nano-particles	**Temperature at the point 14 mm away from center of the probe after 15 min duration**		**Temperature at the point 18 mm away from center of the probe after 15 min duration**	
	Bhargava et al. [32]	**present result ( )*T*1**	**Bhargava et al. [32]**	**present result (*T*2)**
Fe O3 4	–41.3313	–42.1673	–15.2222	–19.3428
Al O2 3	–42.6667 –	–45.3307	–16.1111	–21.7349
Au	43.6667	–46.214	–16.7778	–23.4728

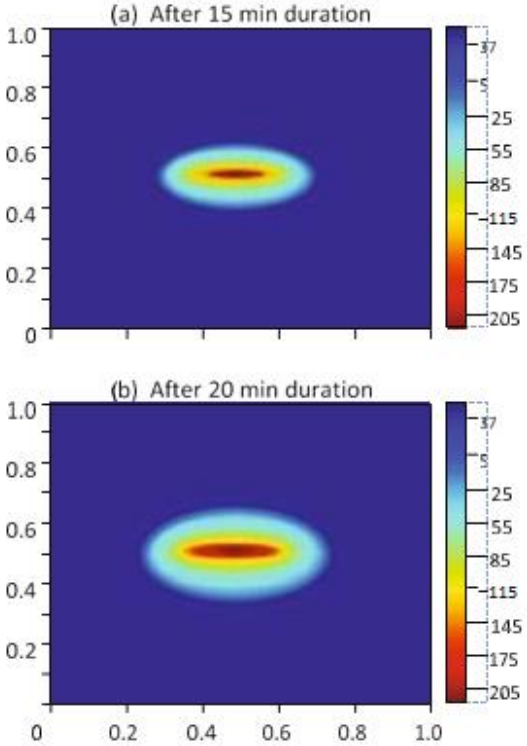

Fig. 2. Temperature Profile inside the computational domain for Al_2O_3 nanoparticles at 4 mm major axis and 2 mm minor axis of cryoprobe for $\phi = 0.20$, $dp = 10$ nm and $\delta = 20$.

ISSN 2394 - 7780

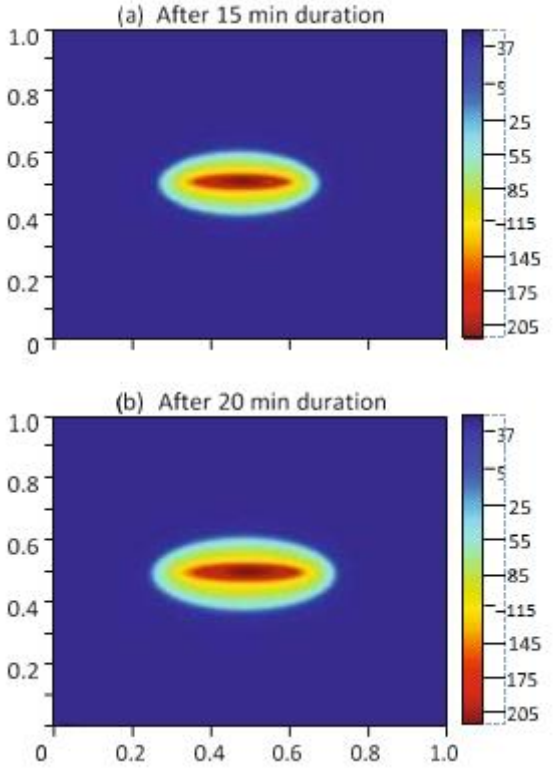

Fig. 3. Temperature Profile inside the computational domain for Fe_3O_4 nanoparticles at 4 mm major axis and 2 mm minor axis of cryoprobe for $\phi = 0.20$, $dp = 10$ nm and $\delta = 20$.

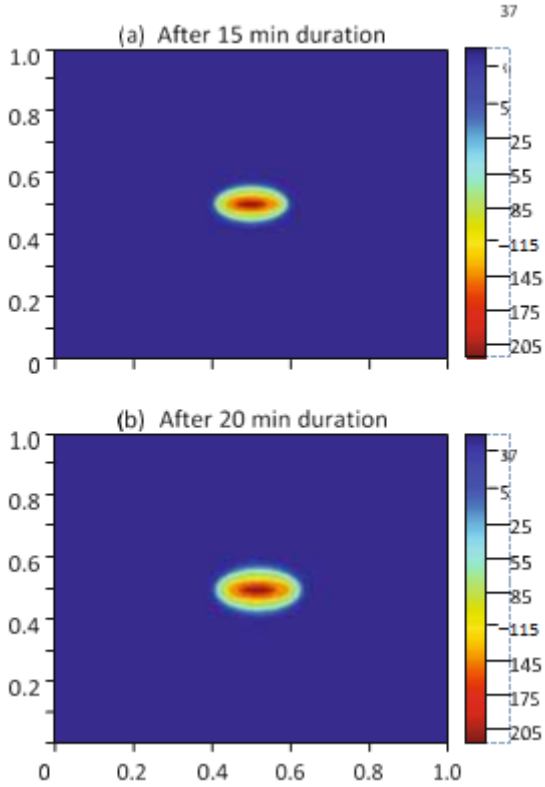

Fig. 4. Temperature Profile inside the computational domain without nanoparticles at 4 mm major axis and 2 mm minor axis of cryoprobe for $\phi = 0.20$, $dp = 10$ nm and $\delta = 20$.

The temperature profile inside computational domain for the freezing of diagnosed tissues after 15 and 20 min in the absence of nanoparticles are computed. The temperature varies near the probe which is not that much efficient to destroy the whole tumor tissues as in the case of nanoparticles. Consequently, nanoparticles have better response in destroying the diseased tissues as compared to probes without nanoparticles.

ISSN 2394 - 7780

In order to make the therapy successful, it is necessary to destroy the tumor tissues completely and efficiently which should not damage the healthy tissues in the vicinity of the diagnosed tissues. The shape of the probe as well as nanoparticle volume fraction has an important role to prevent such kind of dilemma. The elliptic probe is efficient to reduce the damage of healthy tissues in the vicinity of irregular tumor cells. The surgical time is attenuated by employing the larger cryoprobe.

CONCLUSIONS

1. Infusion of the nanoparticles results in increased heat transfer rate. Hence the nanoparticle volume fraction has decisive role in controlling the ice crystal growth in vicinity of diseased tissues.
2. The different nanoparticles having different thermal conductivity, result in varying heat transfer rate. Depending on tumor i.e. malignant or benign tumor, variety of the nanoparticles can be used depending on the required freezing rate.

NOMENCLATURE

a	Semi major axis of probe	δ	Conductivity ratio b
b	Semi minor axis of probe	ϕ	Nanoparticle volume fraction
c	Specific heat capacity	ρ	Density
$h\_$	Latent heat	ω	Perfusion rate k Latent heat
k	Latent heat	***Subscripts***	
Q	External heat source	b	Blood
Qm	Metabolic rate	eff	Effective
t	Time	f	Basefluid
T	Temperature	nf	Nanofluid
X,Y	Coordinate axes	p	Particle
⍺	Penalty Parameter	s	Solid

REFERENCES

1. J. Liu and Z. S. Deng, "Nano-cryosurgery: Advances and challenges," J. Nanosci. Nanotechnol. **9**, 4521–4542 (2009).
2. Y. Hou, Z. Sun, W. Rao, and J. Liu, "Nanoparticle-mediated cryosurgery for tumor therapy," Nanomed: Nanotech. Biol. Med. **14**, 493–506 (2018).
3. J. Rui, K. N. Tatsutani, R. Dahiya, and B. Rubinsky, "Effect of thermal variables on human breast cancer in cryosurgery," BreastCancer Res. Treat. **53**, 185–192 (2021).
4. J. Zhang, G. A. Sandison, J. Y. Murthy, and L. X. Xu, "Numerical simulation for heat transfer in prostate cancer cryosurgery," J. Biomech. Eng. **127** (2), 279–294 (2005).
5. G. Zhao, H. F. Zhang, X. J. Guo, D. W. Luo, and D. Y. Gao, "Effect of blood flow and metabolism on multidimensional heat transfer during cryosurgery," Med. Eng. Phys. **29**, 205–215 (2007).
6. Z. Z. He, X. Xue, J. Xiao, and J. Liu, "Anatomical model-based finite element analysis of the combined cryosurgical and hyperthermic ablation for knee bone tumor," Comput. Methods Programs Biomed. **112**, 356–366 (2023).
7. S. Tanwar and P. Kumari, "X-FEM: An efficient algorithm for simulation of phase transition during prostate cryosurgery," Comput. Math. Appl. **79**, 2119–2132 (2020).
8. S. Singh and R. Bhargava, "Simulation of phase transition during cryosurgical treatment of a tumor tissue loaded with nanoparticles using meshfree approach," J. Heat Transfer **136** (12), 121101 (2014).
9. X. Zhang, S. C. Hossain, G. Zhao, B. Qiu, and X. He, "Two-phase heat transfer model for multiprobe cryosurgery," Appl. Therm. Eng. **113**, 47–57 (2017).
10. E. Li, G. R. Liu, V. Tan, and Z. C. He, "An efficient algorithm for phase change problem in tumor treatment using αFEM," Int. J. Therm. Sci. **49**, 1954–1967 (2010).
11. D. Tanaka, K. Shimada, and Y. Rabin, "Two-phase computerized planning of cryosurgery using bubble-packing and force-field analogy" J. Biomech. Eng. **128** (1), 49–58 (2006).